Two-dimensional clusters of solitary structures in driven optical cavities

Andrei G. Vladimirov,[1] John M. McSloy,[2] Dmitry V. Skryabin,[3,*] and William J. Firth[2]
[1]*Physics Faculty, St. Petersburg State University, St. Petersburg 198904, Russia*
[2]*Department of Physics and Applied Physics, University of Strathclyde, Glasgow G4 0NG, United Kingdom*
[3]*Department of Physics, University of Bath, Bath BA2 7AY, United Kingdom*
(Received 29 August 2001; published 25 March 2002)

Using analytical and numerical approaches we study clusters of the two-dimensional localized structures of light excited in the externally driven optical cavities. Stability and instability properties of clusters of two, three, and four structures are analyzed in detail. We develop a technique for calculation of the expression for the interaction potential through modified Bessel functions that has applicability going beyond the model under consideration. Qualitative differences between stability properties of triangular and square structures are found that emphasize the role of diagonal interactions in the latter.

DOI: 10.1103/PhysRevE.65.046606 PACS number(s): 42.65.Tg, 42.65.Sf, 05.45.Yv

I. INTRODUCTION

Localized structures of light in optical cavities—cavity solitons—have attracted significant attention in recent years. This is largely due to some striking experimental observations [1–4] and the variety of complex and interesting nonlinear phenomena involved in their stability [5–7], interaction [8–11], and control [2,3,5,12]. The last aspect also gives some hope for potential application of these structures for optical processing of information.

Solitons in coherently pumped cavities are typically excited by a localized address pulse of light launched in addition to the sustained pump field [2,3,5]. The latter is transversely-extended, ideally very broad compared to the cavity soliton. Therefore, independent solitons can be created at arbitrary nonoverlapping address locations. If, however, they are excited sufficiently close one to another, then they exert mutual forces due to overlap of their tails, which typically consist of diffraction ripples under a sechlike envelope. Through these forces, cavity solitons can group themselves into geometrical configurations, which will be referred below as *clusters*. Clusters of a different kind can be formed through modulational instability of the background field, where the driving field has a limited beam width, so that it can only support a limited number of cavity solitons.

A thorough theoretical study of cluster formation in models with external driving has been done so far only for one-dimensional (1D) cavity solitons [8–11], with relevant experimental results described in Ref. [4]. Two other experimental papers investigating semiconductor microcavities [3] and single mirror feedback system [13] reported observations of two-dimensional (2D) clusters posing, thereby, the problem of generalization of the theoretical results of Refs. [8–11] to the case of two transverse dimensions.

Of course, the most interesting are those 2D clusters that do not have analogs in the 1D geometry, e.g., triangles, squares, hexagons. This type of structure has been observed in optical cavities both experimentally [3,14] and numerically [15–17]. The problem of formation of clusters from 2D dissipative localized structures has also been addressed in the general context of Swift-Hohenberg models [17–20], reaction-diffusion systems [19,21,22], and vibrated granular layers [20,23]. In dissipative nonlinear optics, analytical approaches closest to ours have been developed in Ref. [16], where an extensive, though qualitative, discussion has been given for 2D clusters of cavity solitons, and in Ref. [24], where pairwise interaction of 2D solitary waves in the complex Ginzburg-Landau equation has been considered using a Hamiltonian-based approach. Note that more attention has been devoted to interaction of localized structures in 1D Ginzburg-Landau-like models [8,25–28].

For Hamiltonian models, also abundant in nonlinear optics, formation of 2D structures with multiple intensity peaks has been quite an active topic of experimental [29,30] and theoretical [29,31,32] research. Interpretation of these structures as bound states of single-hump 2D solitons is to a large extent an open topic with the only known analytical results related to the spiralling of two solitons [33,34].

Below we have chosen to consider a prominent model in the theory of intracavity nonlinear optics, which is a two-level absorbing medium in an optical cavity with photon-life time long compare to the characteristic times of the medium itself [5]. After introduction of the governing equations in the next section, we proceed to describe relevant details of the asymptotic behavior of the tails of the 2D cavity solitons and their neutral (Goldstone) modes. In Sec. IV we develop the theory of existence and stability of clusters and compare its predictions with direct modeling of the dynamical and stationary versions of the governing equations, as well as with numerical linear stability analysis of the clusters. We analyze a variety of structures, providing detailed coverage of the stability properties of clusters of two, three, and four cavity solitons. Let us note here that cavity solitons in the model considered below have a minimal number of possible degrees of freedom, simply their position coordinates in the transverse plane. 2D clusters of solitary waves having phase [24,26–28,35] and other [10] degrees of freedom are interesting subjects not treated in the present work.

*Corresponding author. Email address: d.v.skryabin@bath.ac.uk

II. MODEL EQUATIONS

We consider the model [5]

$$\partial_t E = i\nabla_\perp^2 E - E\left[1 + i\theta + \frac{2C}{1+|E|^2}\right] + E_I \tag{1}$$

describing dynamics of the slowly varying amplitude E of an electromagnetic wave inside a coherently pumped optical cavity with fast saturable absorber. Here θ is the detuning of the pump frequency from the cavity resonance, normalized to the decay time of a photon, $2C$ parametrizes the nonlinear absorption, and E_I is the (spatially independent) amplitude of the driving field. t is the time measured in units of the photon decay time in the empty cavity ($C=0$). We assume that there is no dispersive contribution to the nonlinear response, which corresponds to that of a two-level atomic medium in which the detuning of the pump frequency from the atomic resonance is zero. $\nabla_\perp^2$ is the transverse Laplacian: $\nabla_\perp = \mathbf{j}_x\partial_x + \mathbf{j}_y\partial_y$.

The spatially homogeneous time-independent solution of Eqs. (1), $E=E_0$, serves as a background for localized structures [5], clusters of which we are going to study. For appropriate parameters, including those we will adopt, E_0 is unique. It is convenient for us to substitute $E=E_0[1+S(x,y,t)]$ into Eq. (1). In terms of S, cavity solitons sit on zero background. S obeys

$$i\partial_t S + \nabla_\perp^2 S = ig(S,S^*),$$

$$g \equiv -(1+i\theta)S + \frac{2C}{1+|E_0|^2} - \frac{2C(1+S)}{1+|E_0|^2(1+S)(1+S^*)}. \tag{2}$$

Introducing the vector function $\vec{\psi}=(S,S^*)^T$ we rewrite Eq. (2) in a form convenient for our analysis

$$i\partial_t\vec{\psi} + \hat{D}\nabla_\perp^2\vec{\psi} = \hat{P}[0]\vec{\psi} + i\vec{\mathcal{N}}[\vec{\psi}], \tag{3}$$

where

$$\hat{D} = \begin{bmatrix} 1 & 0 \\ 0 & -1 \end{bmatrix}, \quad \hat{P}[\vec{\psi}] = i\begin{bmatrix} \partial_S g & \partial_{S^*} g \\ \partial_S g^* & \partial_{S^*} g^* \end{bmatrix}. \tag{4}$$

We have separated the linear and nonlinear terms on the right-hand side of Eq. (3): $\hat{P}[0] \equiv \hat{P}[\vec{\psi}=\vec{0}]$ and function $i\vec{\mathcal{N}}[\vec{\psi}] = i(g,g^*)^T - \hat{P}[0]\vec{\psi}$. Here and below vectors in the (x,y) plane are shown by bold symbols and other vectors associated with two-component structure of our field are marked by arrows. The definitions of the scalar products used below are: for vectors $\vec{U}_{1,2}=(U_{1,2},U_{1,2}^*)^T$, we define $(\vec{U}_1\cdot\vec{U}_2) \equiv 2\,\mathrm{Re}(U_1^* U_2)$, then $\langle\vec{U}_1|\vec{U}_2\rangle \equiv \int_{-\infty}^{\infty}dx\int_{-\infty}^{\infty}dy(\vec{U}_1\cdot\vec{U}_2)$, and for two vectors in the (x,y) plane $(\mathbf{a}\cdot\mathbf{b}) \equiv a_x b_x + a_y b_y$.

It is important for the following that Eq. (3) is invariant under translations

$$\mathbf{r} \to \mathbf{r} + \mathbf{r}_0, \quad \mathbf{r}=(x,y), \tag{5}$$

and rotations around the origin

$$\mathbf{r} \to \begin{pmatrix} \cos\delta & \sin\delta \\ -\sin\delta & \cos\delta \end{pmatrix}\mathbf{r} \tag{6}$$

in the (x,y) plane. Here $\delta = \arg(x_0 + iy_0)$ is an arbitrary angle of rotation.

III. PROPERTIES OF ISOLATED CAVITY SOLITONS

A. Tails of the cavity solitons

Equation (3) has multiple families of cavity solitons existing in the vicinity of the bistability region of E_0 [5,17]. We will be interested below in the interaction of the simplest, radially symmetric, cavity solitons, $S=S_s(r)$, obeying

$$\hat{D}\left(\frac{d^2}{dr^2} + \frac{1}{r}\frac{d}{dr}\right)\vec{\psi}_s = \hat{P}[0]\vec{\psi}_s + i\vec{\mathcal{N}}[\vec{\psi}_s], \tag{7}$$

where $r=\sqrt{x^2+y^2}$ and $\vec{\psi}_s(r\to\infty)\to 0$. In the context of the cluster formation the behavior of the soliton tails is particularly important. Because function $\vec{\mathcal{N}} \sim O(|\vec{\psi}_s|^2)$, it becomes negligible at large r as $S\to 0$. In this limit, Eq. (7) reduces to an explicitly solvable linear problem and the asymptotic behavior of the tails of a cavity soliton positioned at $\mathbf{r}=0$ is given by, cf. Ref. [5],

$$\vec{\psi}_s(r\to\infty) \to b\vec{\mathcal{B}}K_0(kr) + b^*\hat{\tau}\vec{\mathcal{B}}^* K_0^*(kr), \tag{8}$$

where

$$\hat{\tau} = \begin{pmatrix} 0 & 1 \\ 1 & 0 \end{pmatrix} \tag{9}$$

is the transposition matrix, k and $\vec{\mathcal{B}}$ are an eigenvalue and eigenvector of the generalized eigenvalue problem (EVP)

$$\hat{P}[0]\vec{\mathcal{B}} = k^2\hat{D}\vec{\mathcal{B}} \tag{10}$$

with

$$k^2 = \theta \pm i\sqrt{\left(1 + \frac{2C}{(1+|E_0|^2)^2}\right)^2 - \frac{4C^2|E_0|^4}{(1+|E_0|^2)^4}}. \tag{11}$$

K_0 and K_1 (see below) are modified Bessel functions of zero and first orders, respectively. $\hat{D}$ and $\hat{P}[0]$ are 2×2 matrices and, therefore, all eigenvalues of Eq. (10) are included in the set $\pm k$ and $\pm k^*$. From Eq. (8) we must choose $\mathrm{Re}\,k>0$, in order that $\vec{\psi}_s$ vanish as $r\to\infty$. In the parameter range where $S=0$ is stable, which is a necessary condition for the existence of stable cavity solitons, $\mathrm{Im}\,k\neq 0$ and, therefore, the tail of the soliton is oscillatory. The complex constant b has to be found numerically, e.g., by matching of Eq. (8) with an exact soliton solution of Eq. (7). This can be efficiently done using the shooting method, which was intro-

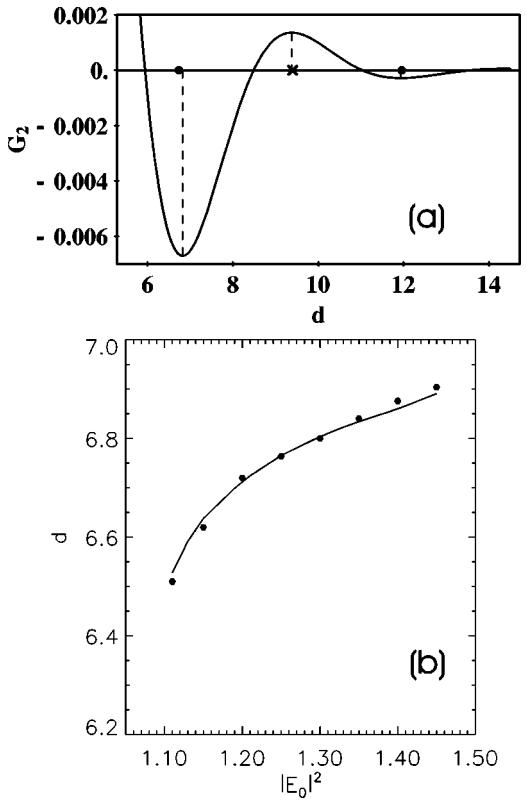

FIG. 1. (a) Potential function G_2 describing two cavity soliton interaction. Minima of this function correspond to stable stationary two cavity soliton clusters. Dots (crosses) on the d axis indicate the intersoliton distances for stable (unstable) clusters calculated numerically using the Newton method. The parameters of Eq. (2) are $C=5.4$, $\theta=-1.2$, and $|E_0|^2=1.33$. This corresponds to $k=0.565-1.232i$ and $ab/\gamma=-0.184-0.080i$ in Eq. (24). (b) First stable separation distance as a function of $|E_0|^2$ for the two-soliton clusters θ and C as above. Dots indicate numerical and full line theoretical results.

duced in the given context in Ref. [5]. The phase of b determines the positions of the zeros of the real and imaginary parts of the soliton tail.

B. Neutral modes

One of the main goals of our asymptotic theory is reduction of the partial differential equation (3) to a set of ordinary differential equations for some *order* parameters of the interacting solitons. These order parameters are the amplitudes of those eigenmodes of the cavity soliton spectrum that are most easily excited by perturbations. The latter in our case come from the overlap of the tails of neighboring solitons. The dimensionality of the phase space of the reduced problem is determined by the number of critical modes times the number of interacting solitons. To find these modes we need to consider the linear EVP associated with an isolated cavity soliton.

In order to do this we substitute the ansatz $\vec{\psi}=\vec{\psi}_s(r)+\vec{\delta\psi}(x,y,t)$ into Eq. (3) and, disregarding all terms nonlinear in $\vec{\delta\psi}$, derive

$$\partial_t\vec{\delta\psi}=\hat{\mathcal{L}}\vec{\delta\psi}, \tag{12}$$

where

$$\hat{\mathcal{L}}[\vec{\psi}_s]=i\hat{D}\nabla_\perp^2-i\hat{P}[\vec{\psi}_s]. \tag{13}$$

Applying infinitesimal translations (5) to the cavity soliton solution we generate two neutral (*translational*) modes $\vec{\mathcal{U}}^{(x)}=\partial_x\vec{\psi}_s=(x/r)\vec{\mathcal{U}}^{(r)}$ and $\vec{\mathcal{U}}^{(y)}=\partial_y\vec{\psi}_s=(y/r)\vec{\mathcal{U}}^{(r)}$, with $\vec{\mathcal{U}}^{(r)}=\partial_r\vec{\psi}_s$. These modes obey $\hat{\mathcal{L}}\vec{\mathcal{U}}^{(x,y)}=0$. Application of the infinitesimal rotations (6) around the cavity soliton center generates zero eigenmode: $\partial_\delta\vec{\psi}_s=0$, $\delta=arg(x+iy)$. Note that rotational symmetry becomes broken for clusters, which are therefore have an extra neutral (*rotational*) mode in their spectra. The asymptotic behavior of the tails of the neutral modes of $\hat{\mathcal{L}}$ can be easily obtained using Eq. (8) and the identity $\partial_r K_0(r)=-K_1(r)$.

The neutral modes $\vec{\mathcal{V}}$ of the adjoint operator $\hat{\mathcal{L}}^\dagger$, obeying $\hat{\mathcal{L}}^\dagger\vec{\mathcal{V}}=0$, are required when solvability conditions are applied to equations appearing at different stages of the asymptotic expansions performed in Sec. IV. The spectra of $\hat{\mathcal{L}}$ and $\hat{\mathcal{L}}^\dagger$ are identical, but their eigenmodes are not. The neutral modes of $\hat{\mathcal{L}}^\dagger$ corresponding to the translational symmetry are $\vec{\mathcal{V}}^{(x)}=x\vec{\mathcal{V}}^{(r)}/r$, $\vec{\mathcal{V}}^{(y)}=y\vec{\mathcal{V}}^{(r)}/r$, where $\vec{\mathcal{V}}^{(r)}$ has the following asymptotic behavior:

$$\vec{\mathcal{V}}^{(r)}(r\to\infty)\to a^*\vec{\mathcal{A}}K_1^*(kr)+a\hat{\tau}\vec{\mathcal{A}}^*K_1(kr). \tag{14}$$

Here a is a constant coefficient with arbitrary absolute value but a fixed phase, which can be found by matching of the zeros of Eq. (14) and of the exact neutral modes of $\hat{\mathcal{L}}^\dagger$. $\vec{\mathcal{A}}$ is an eigenvector of the EVP,

$$\hat{P}^\dagger[0]\vec{\mathcal{A}}=k^{*2}\hat{D}\vec{\mathcal{A}}. \tag{15}$$

IV. ASYMPTOTIC THEORY OF CLUSTER FORMATION

We start by considering the simplest example of two interacting cavity solitons. Once equations for two are derived, they can be straightforwardly generalized for an arbitrary number of solitons. We assume that in the leading approximation the solution of Eqs. (3) can be represented as a superposition of two independent cavity solitons:

$$\vec{\psi}=\vec{\psi}_{s1}+\vec{\psi}_{s2}+\vec{\mathcal{E}}+O(\epsilon^{3/2}), \tag{16}$$

where $\vec{\psi}_{sn}=\vec{\psi}_s(|\mathbf{r}_n|)$ are the two cavity solitons located at $\mathbf{R}_n=\mathbf{j}_x X_n+\mathbf{j}_y Y_n$, $n=1,2$, $\mathbf{r}_n=\mathbf{r}-\mathbf{R}_n$ and $\vec{\mathcal{E}}$ is a correction due to nonlinearity, describing deviations of the two cavity soliton solution from the linear superposition of the individual solitons. The soliton positions are assumed to be slowly varying functions of time $\partial_t\mathbf{R}_n\sim O(\epsilon)$, where $\epsilon\ll 1$ is a measure of the smallness of the overlap of the soliton tails.

Substituting Eq. (16) into Eq. (3) we find at order ϵ

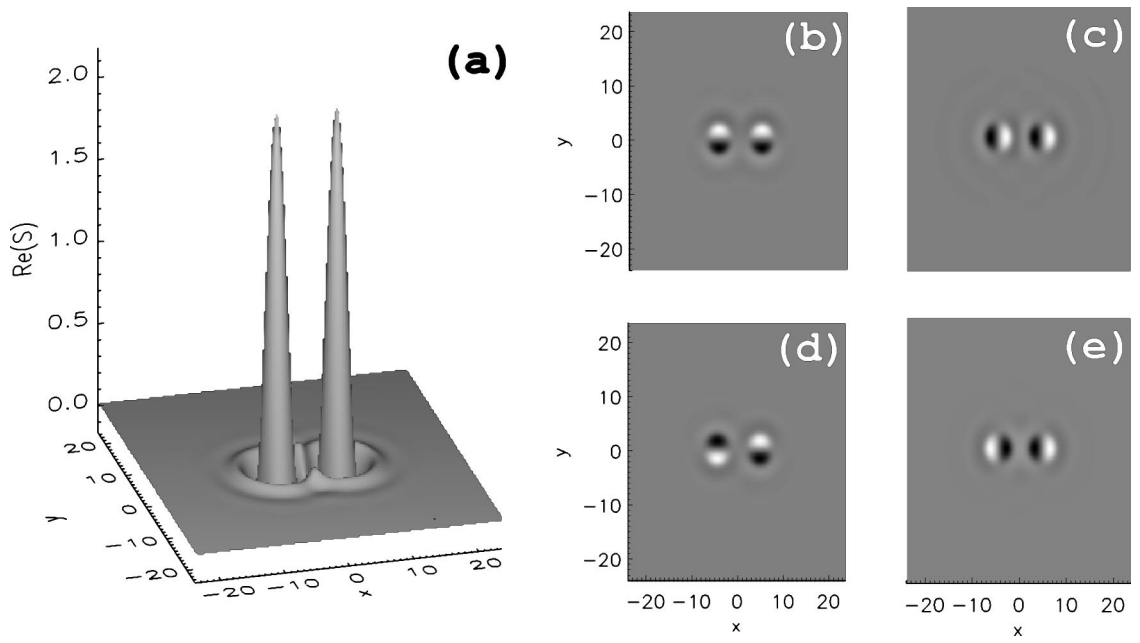

FIG. 2. Real part of field S for (a) the $N=2$ unstable cluster, and its respective neutral (b), (c), (d) and unstable (e) modes. Parameters as in Fig. 1(a).

$$\hat{\mathcal{L}}[\vec{\psi}_{s1}+\vec{\psi}_{s2}]\vec{\mathcal{E}}=-\vec{\mathcal{U}}_1^{(r)}\left(\frac{\mathbf{r}_1}{r_1}\cdot\partial_t\mathbf{R}_1\right)-\vec{\mathcal{U}}_2^{(r)}\left(\frac{\mathbf{r}_2}{r_2}\cdot\partial_t\mathbf{R}_2\right)-\vec{\mathcal{I}}, \tag{17}$$

where

$$\vec{\mathcal{I}}=\vec{\mathcal{N}}[\vec{\psi}_{s1}+\vec{\psi}_{s2}]-\vec{\mathcal{N}}[\vec{\psi}_{s1}]-\vec{\mathcal{N}}[\vec{\psi}_{s2}], \tag{18}$$

and $\vec{\mathcal{U}}_n^{(r)}=\vec{\mathcal{U}}^{(r)}(|\mathbf{r}_n|)$. Solvability of Eq. (17) requires that its right-hand side is orthogonal to the neutral modes of $\hat{\mathcal{L}}^{\dagger}$, which yields

$$\gamma\partial_t\mathbf{R}_n=-\left\langle\frac{\mathbf{r}_n}{r_n}\vec{\mathcal{V}}_n^{(r)}\middle|\vec{\mathcal{I}}\right\rangle. \tag{19}$$

Here $\vec{\mathcal{V}}_n^{(r)}=\vec{\mathcal{V}}^{(r)}(|\mathbf{r}_n|)$, and $2\gamma=2\langle\vec{\mathcal{V}}_n^{(x,y)}|\vec{\mathcal{U}}_n^{(x,y)}\rangle=\langle\vec{\mathcal{V}}_n^{(r)}|\vec{\mathcal{U}}_n^{(r)}\rangle>0$. The soliton velocity under a given perturbation is inversely proportional to γ, which plays the role of a viscosity coefficient.

Now we briefly outline the analytical calculation of the overlap integrals $\langle(\mathbf{r}_n/r_n)\vec{\mathcal{V}}_n^{(r)}|\vec{\mathcal{I}}\rangle$. Let $R_{21}=|\mathbf{R}_2-\mathbf{R}_1|$ be the distance between the cavity solitons. Without loss of generality we can assume that their intensity maxima are located at the points $(-R_{21}/2,0)$ and $(R_{21}/2,0)$ lying on the x axis of the (x,y) plane. Then the scalar product in the overlap integrals can be represented as

$$\left\langle\frac{\mathbf{r}_n}{r_n}\vec{\mathcal{V}}_n\middle|\vec{\mathcal{I}}\right\rangle=\left\langle\frac{\mathbf{r}_n}{r_n}\vec{\mathcal{V}}_n\middle|\vec{\mathcal{I}}\right\rangle_n+\left\langle\frac{\mathbf{r}_n}{r_n}\vec{\mathcal{V}}_n\middle|\vec{\mathcal{I}}\right\rangle_m, \tag{20}$$

where $m=1,2$, $m\neq n$ and $\langle|\rangle_n$ means that the corresponding integral is calculated over the half-plane $(-1)^n x>0$.

If the intensity maximum of the localized solution $\vec{\psi}_{sn}$ lies in the half-plane $(-1)^n x>0$, then, inside this region, the absolute value of the solution $\vec{\psi}_{sm}$ is small compared to that of $\vec{\psi}_{sn}$. This smallness can be used to make the following asymptotic estimates:

$$\vec{\mathcal{N}}[\vec{\psi}_{s1}+\vec{\psi}_{s2}]=\vec{\mathcal{N}}[\vec{\psi}_{sn}]+(\hat{\mathcal{L}}[\vec{\psi}_{sn}]-\hat{\mathcal{L}}[0])\vec{\psi}_{sm}+O(\epsilon^{3/2}), \tag{21}$$

and $\vec{\mathcal{N}}[\vec{\psi}_{sm}]=O(\epsilon^{3/2})$. Substituting Eq. (21) into Eq. (18) we get

$$\vec{\mathcal{I}}=(\hat{\mathcal{L}}[\vec{\psi}_{sn}]-\hat{\mathcal{L}}[0])\vec{\psi}_{sm}+O(\epsilon^{3/2})=\hat{\mathcal{L}}[\vec{\psi}_{sn}]\vec{\psi}_{sm}+O(\epsilon^{3/2}). \tag{22}$$

Up to the leading order terms $\vec{\mathcal{I}}$ is obviously linear in $\vec{\psi}_{sm}$ and, therefore, in the case of more than two solitons $\vec{\mathcal{I}}$ can be estimated as the sum of the right-hand side of Eq. (22) over m. Using Eq. (22) we calculate all integrals in Eq. (20) explicitly (see Appendix for details) and finally derive equations governing the motion of N interacting cavity solitons

$$\gamma\partial_t\mathbf{R}_n=-4\pi\sum_{m=1,m\neq n}^{N}\frac{\mathbf{R}_{nm}}{R_{nm}}\mathrm{Im}[abK_1(kR_{nm})]. \tag{23}$$

From a formal point of view this system of equations is valid providing that every term on the right-hand side has order of ϵ. In other words, all cavity solitons should be located at approximately the same distance from one another. Practically, however, Eq. (23), taking into account only the leading order contributions from all the pairwise interactions, gives a good approximation for intersoliton distances in a cluster even when these distances are significantly different.

It can be shown that neglecting the $O(\epsilon^{3/2})$ corrections in Eq. (16) cannot alter stability of a stable cluster. In particular, it cannot lead to appearance of extra neutral modes in the

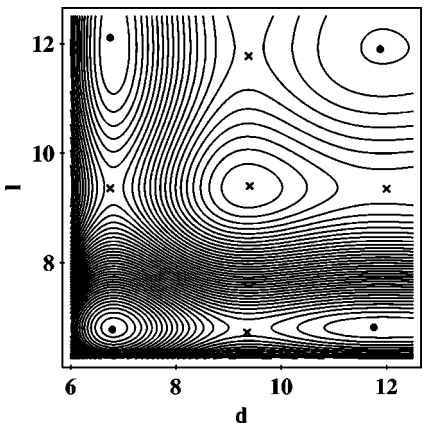

FIG. 3. Contour lines of potential function $G_3(l,d)$ describing isosceles triangles with the sides l, l, and $d<2l$. Dots (crosses) correspond to stable (unstable) clusters of three cavity solitons found by the Newton method. Parameters as in Fig. 1(a).

cluster spectrum. The latter does happen, however, if some pairwise interactions themselves are neglected, even if they are relatively weak. Such an example arises in the case of the stability of four-soliton clusters in Sec. IV C.

Equation. (23) can be easily transformed into the gradient form

$$\partial_t \mathbf{R}_n = \nabla_{\mathbf{R}_n} G_N, \tag{24}$$

$$G_N = 2\pi \,\mathrm{Im}\left[\frac{ab}{\gamma k}\sum_{j\neq l}^{N} K_0(kR_{jl})\right],$$

where $\nabla_{\mathbf{R}_n} = \mathbf{j}_x \partial_{X_n} + \mathbf{j}_y \partial_{Y_n}$. Thus in our model the tails of any number N of cavity solitons create an effective potential G_N and a system of N scattered solitons will evolve towards a state where the solitons' positions correspond to a minimum of the potential G_N. Clearly the interaction between a given pair of cavity solitons is independent of any other cavity solitons present. The net force on a given cavity soliton is simply the vector sum its interaction forces with every other soliton. Thus the interaction forces between solitons in an externally driven cavity obey the same principle of superposition as, e.g., Coulomb or gravitational forces. Note, however, that on the left-hand side of Eq. (23) we have the velocity, not the acceleration, of the nth soliton, and so the forces acting between the cavity solitons are Aristotelian rather than Newtonian.

For $|k|R_{nm} \gg 1$ the oscillatory nature of the interaction forces due to the soliton tails becomes obvious from the approximation

$$K_0(kR) \simeq \left[\frac{\pi}{2|k|R}\right]^{1/2} e^{-kR - i\arg(k)/2}\left[1 + O\left(\frac{1}{|k|R}\right)\right], \tag{25}$$

which gives

$$G_N = \frac{G_0}{2}\sum_{j\neq l}^{N} \frac{e^{-\mathrm{Re}(k)R_{jl}}\cos[-\mathrm{Im}(k)R_{jl} + \phi]}{\sqrt{R_{jl}}}, \tag{26}$$

where $G_0 = (2\pi/|k|)^{3/2}(|ab|/\gamma)|$ and $\phi = \arg(ab) - (3/4)\arg(k)$.

We are not aware of any previous work in which the interaction potential of 2D localized structures has been obtained in explicit form based on Bessel functions, see Eqs. (23), (24) and Appendix. Approximations similar to Eq. (25), are usually applied from the very beginning, when calculating the asymptotic behavior (8) of the soliton tails [18,24].

A. Clusters of two cavity solitons

For two solitons, system (23) can be reduced to separate equations for the relative, $\mathbf{d} = \mathbf{R}_1 - \mathbf{R}_2$, and absolute, $(\mathbf{R}_1 + \mathbf{R}_2)/2$, positions, namely,

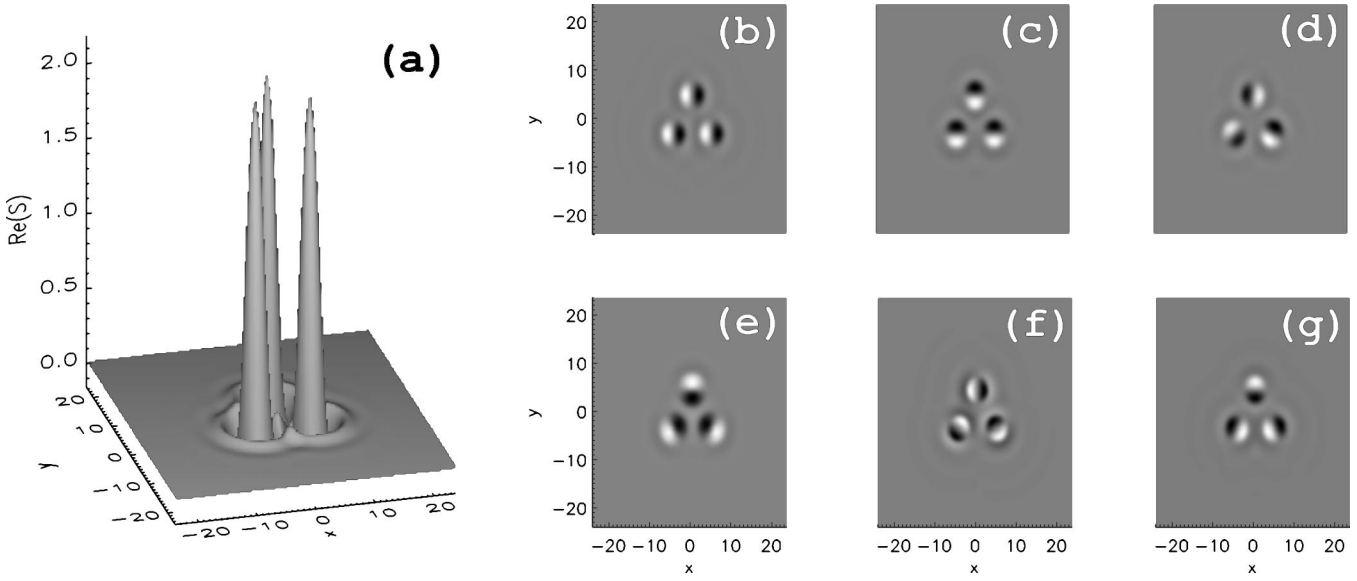

FIG. 4. Real part of field S for (a) the $N=3$ unstable cluster, and its respective neutral (b), (c), (d) and unstable (e), (f), (g) modes. Parameters as in Fig. 1(a).

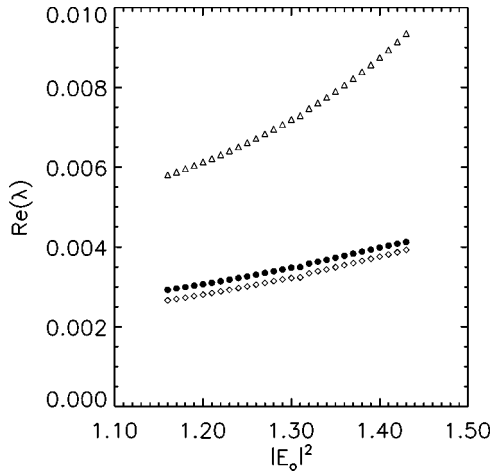

FIG. 5. Growth rates of unstable modes vs $|E_0|^2$ for an $N=3$ cluster of the type shown in Fig. 4. Triangles, dots, and diamonds, respectively, denote eigenmodes shown in panels (e), (f), and (g) of Fig. 4.

$$\partial_t d = 2\partial_d G_2, \quad G_2(d) = \frac{4\pi}{\gamma}\mathrm{Im}\left[\frac{ab}{k}K_0(kd)\right], \tag{27}$$

$$\partial_t \arg\{(\mathbf{j}_x\cdot\mathbf{d}) + i(\mathbf{j}_y\cdot\mathbf{d})\} = 0, \tag{28}$$

$$\partial_t(\mathbf{R}_1+\mathbf{R}_2)/2 = 0, \tag{29}$$

where $d=|\mathbf{d}|$. Thus a system of two two-dimensional solitons has four effective degrees of freedom. Three of them are neutral and only one, which is the distance d between the soliton centers, governs possible instability scenarios. A plot of the function G_2 for typical parameters is shown in Fig. 1(a). It indicates that stable [minima of $G_2(d)$] and unstable clusters [maxima of $G_2(d)$] alternate with increasing d.

To check our theoretical predictions we have prepared several numerical programs. First, direct modeling of Eq. (2) using the standard split-step approach. Second, a Newton-method-based program solving Eq. (7) (able to find both stable and unstable soliton clusters). Third, an Arnoldi-method-based [36] program that calculates the spectrum of the operator $\hat{\mathcal{L}}$ for stationary solutions found by the Newton method. Fourth, the already mentioned above high-accuracy shooting method to calculate the radial profiles of the solitons and neutral modes of the operators $\hat{\mathcal{L}}$ and $\hat{\mathcal{L}}^\dagger$. The latter were used to evaluate the quantities γ, a, and b that enter Eqs. (24). In all our numerical calculations we fix $\theta=-1.2$ and $C=5.4$.

Dots (crosses) in Fig. 1(a) show distances for stable (unstable) cavity soliton pairs found by the Newton method, indicating excellent agreement between the numerical and theoretical predictions. The latter give for the first two stable distances $d\simeq 6.81$ and $d\simeq 11.93$ and for the unstable distance between them $d\simeq 9.38$, for our selected system parameters. Figure 1(b), showing dependence of the first stable separation distance vs $|E_0|^2$, further facilitates comparison between numerical and theoretical predictions. Figure 2 shows the numerically computed unstable cluster with $d\simeq 9.38$, and four of the eigenmodes associated with the eigenvalues of $\hat{\mathcal{L}}$ with largest real parts. Looking for small perturbations of the equilibria, $\partial_d G_2=0$, of Eqs. (27)–(29) in the form $\sim e^{\lambda t}$ we find the characteristic polynomial

$$\lambda^3(\lambda - 2\partial_d^2 G_2) = 0, \tag{30}$$

where three zero roots correspond to the neutral modes. Neutral modes in Figs. 2(b), 2(c) linked to Eq. (29) are translational ones, $\partial_{x,y}(\vec{\psi}_{s1}+\vec{\psi}_{s2})+O(\epsilon)$. The rotational neutral mode in Fig. 2(d) corresponds to Eq. (28) and is given by $\partial_\delta(\vec{\psi}_{s1}+\vec{\psi}_{s2})+O(\epsilon)$. The only unstable mode, $\partial_x(\vec{\psi}_{s1}-\vec{\psi}_{s2})+O(\epsilon)$, is shown in Fig. 2(e). Its excitation changes the distance between the interacting solitons, transforming an unstable cluster into one of the neighboring stable ones. More generally, any cluster of N cavity solitons has $2N$ de-

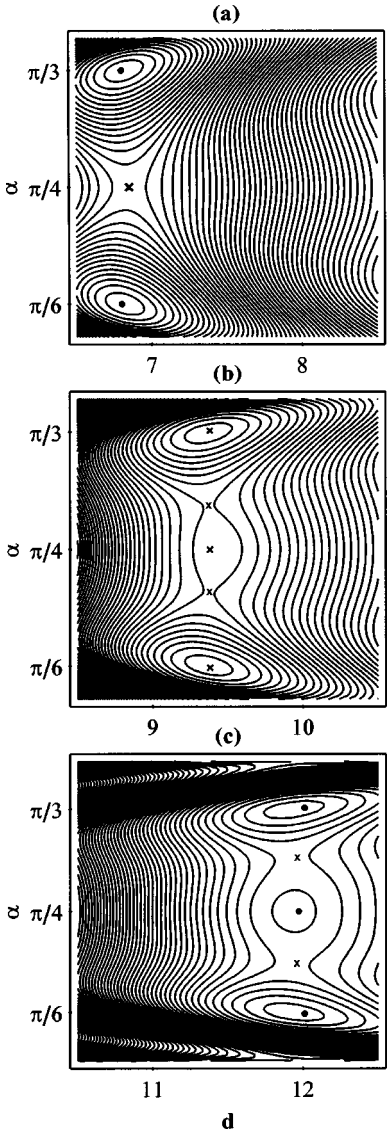

FIG. 6. Potential function $G_4(d,\alpha)$ describing a rhomboid cluster with sides d and angle 2α between the sides. (a), (b), (c) panels cover three successive intervals of d. Dots (crosses) indicate the stable (unstable) clusters calculated numerically using the Newton method. Parameters as in Fig. 1(a).

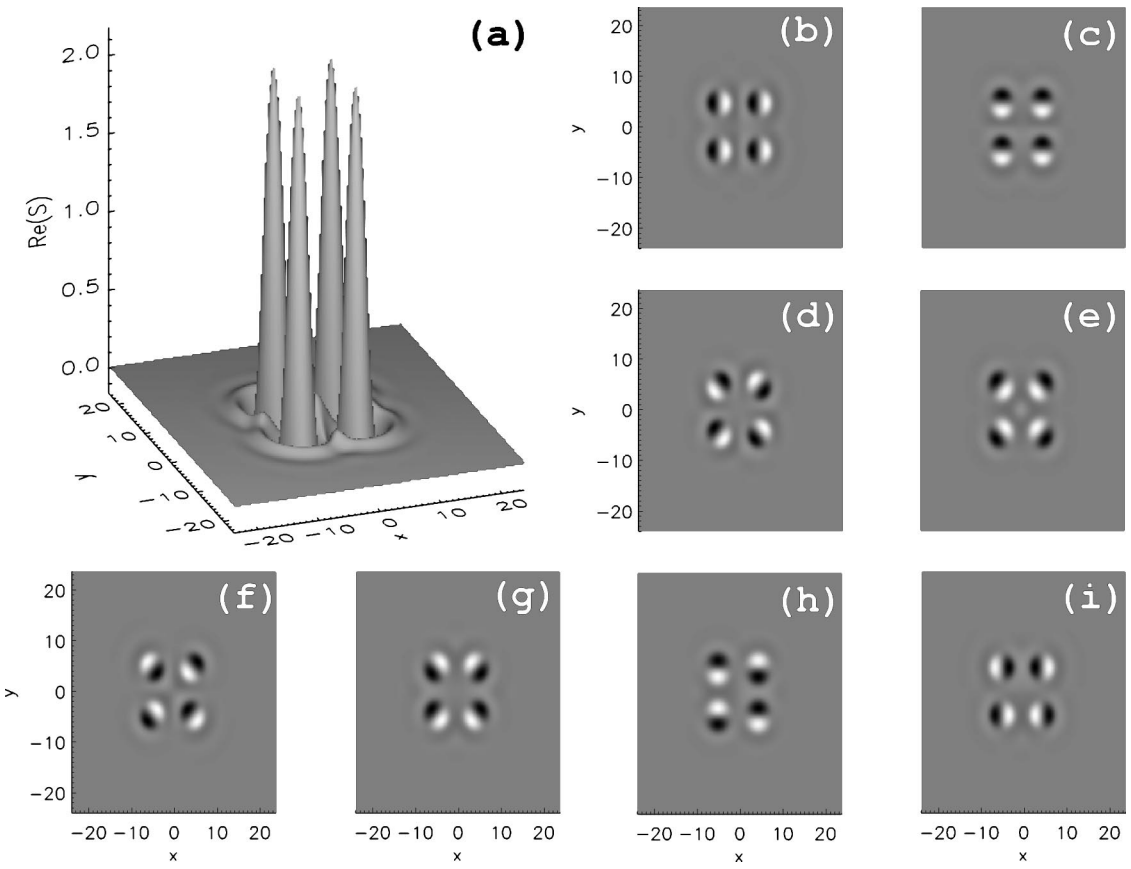

FIG. 7. Real part of field S for (a) the $N=4$ unstable cluster, and its respective neutral (b), (c), (d) and unstable (e), (f), (g), (h), (i) modes. Parameters as in Fig. 1(a).

grees of freedom. Three of those are always neutral (two translational and one rotational), while the others can be either stable or not.

B. Clusters of three cavity solitons

It is clear from Eqs. (23), (24) that for clusters of three or more cavity solitons the interaction potential is just the sum of pairwise potentials, with the pairs of solitons exerting equal and opposite forces on each other directed along the line joining them. It follows that for a triangular configuration of three solitons that the only possible stationary configurations, i.e., when the total force on each soliton is equal to zero, are those when each pairwise interaction is exactly balanced. Simple visual representation of the stability of triangular clusters is possible when the cluster can be fully characterized by just two geometrical parameters, e.g., the case of isosceles triangles, with two sides of length l and the third side of length d. The level lines of G_3 for this case are shown in Fig. 3. Stationary triangular clusters are predicted where $\partial_l G_2(l)=0$ and $\partial_d G_2(d)=0$. The marks in this figure indicate the three-soliton clusters calculated numerically using the Newton's method, and again there is very good agreement with the extrema of G_3. Each of the stable clusters indicated by dots corresponds closely to a minimum of the potential function G_3. Unstable clusters are indicated by crosses, and each corresponds to a maximum or saddle of G_3. The numerically calculated distances d and l are only slightly different from those corresponding to critical points of the theoretical potential given by Eq. (24). However, we expect that this discrepancy can be mainly attributed to the errors of the numerical solutions, and to the less extent to the approximations of the analytical technique.

An arbitrary triangle is stable if it consists of three stable two-soliton clusters. This is because only possible transformations of the triangles, different from the symmetry transformations (5)–(6), are stretching or shortening of the sides. Therefore, if all side lengths correspond to stable two-soliton clusters, then the whole triangle is stable. This can be proved through linear stability analysis of Eq. (23) for $N=3$. Though the general case results in a rather cumbersome expression, it can be handled with a computer algebra package. We will see in the next subsection that four-soliton clusters are qualitatively different from three-soliton ones, because for $N=4$ diagonal interactions play an important role.

The numerically computed equilateral cluster of three solitons for $d\simeq 9.38$ is shown in Fig. 4(a). It has six degrees of freedom, three of which are neutral, see Figs. 4(b)–4(d). The other three are unstable because all three side interactions are obviously unstable for the chosen distance, see Fig. 1(a). In Fig. 5 we show numerically computed dependencies of all three unstable eigenvalues vs pump parameter showing that dominating instability scenario is the dilation transfor-

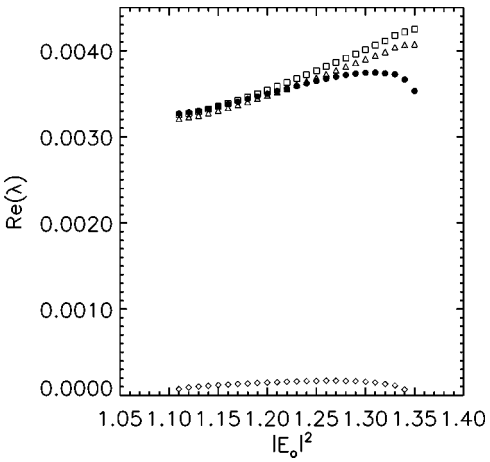

FIG. 8. Growth rates of unstable modes vs $|E_0|^2$ for an $N=4$ square cluster of the type shown in Fig. 7. Dots, diamonds, squares, and triangles, respectively, denote eigenmodes of the form shown in panels (e), (f), (g), and (h), (i) of Fig. 7.

mation, see the eigenmode in Fig. 4(e). This mode retains the shape of the cluster, while transforming the unstable equilateral triangle into one of the stable ones. The eigenmodes corresponding to the transition to the isosceles triangle, see Fig. 4(g), and to a triangle with all sides different, see Fig. 4(f), have smaller growth rates throughout the entire region of existence.

C. Clusters of four and more cavity solitons

We will focus here on the simplest and most important cases of square and rhomboidal clusters. An immediate question, which arises in this context is whether interaction along the diagonals of the square and rhombus are relevant in Eq. (23) or not. But it is clear that if we disregard interaction forces along the diagonals any square is neutrally stable with respect to perturbations transforming it into the rhombus with the same side length. To make a rigid square we need to take into account both diagonal interactions. For a rhombus it is enough to include into Eq. (23) interaction along the shortest diagonal only.

As for the case of triangles, we present here numerical calculations and qualitative discussion of the stability properties of rhombuses and squares supported by the level plots of the potential G_4, see Fig. 6. To parametrize the interaction potential in this case we use parameters d, which is the side length, and α, which is the half angle between the two sides. Stable and unstable clusters calculated numerically by Newton method are shown by dots and crosses, respectively. Despite diagonal forces being significant, they are still weaker than forces acting along the sides. Therefore, the equilibrium distances between neighboring solitons are quite close to those found from the analysis of side interactions only. Degrees of freedom corresponding to the transformation of a rhomboidal cluster into rectangular, trapezoid, or quadrangle are obviously not covered by the plot in Fig. 6. However, their inclusion would not alter the stability of those clusters which are minima in Fig. 6. This is because the limitations of Fig. 6 are related to degrees of freedom corresponding to the change of the length of one side with respect to another. The latter, however, is determined from the pairwise side interactions only. At the same time stability due to degrees of freedom associated with stretching of the diagonal is taken into account through the angle α.

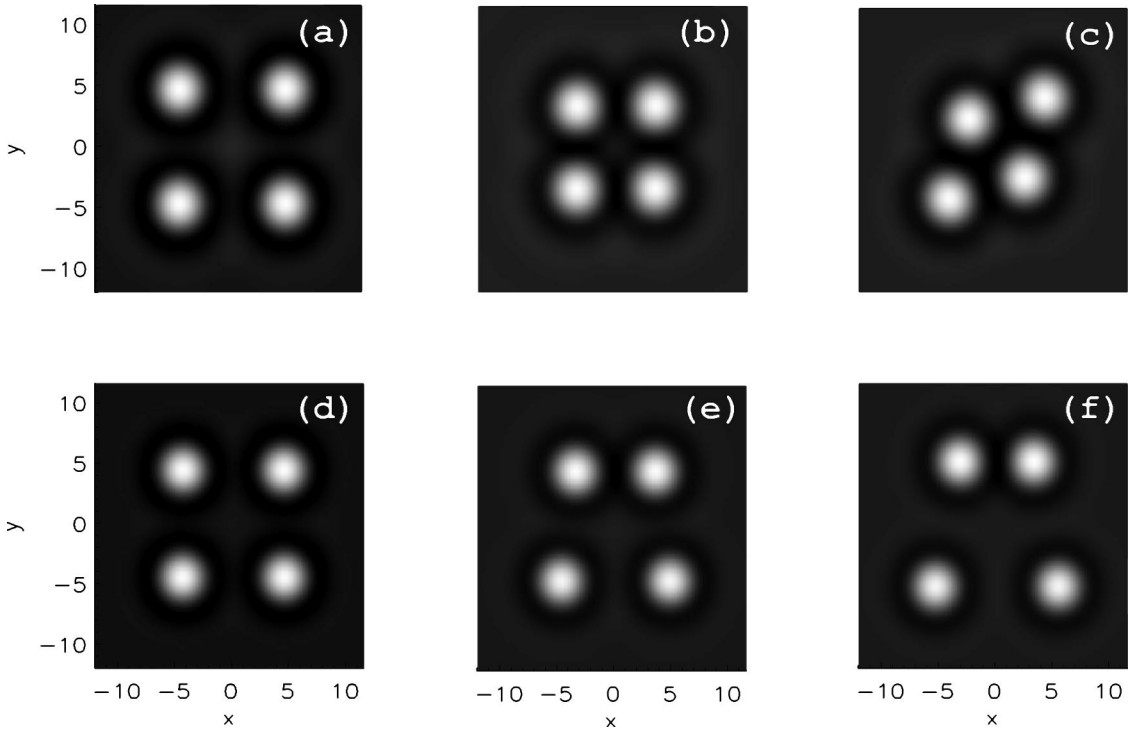

FIG. 9. Evolution of an unstable square (cf. Fig. 7), perturbed by noise at pump values $|E_0|^2=1.15$ (a)–(c) and $|E_0|^2=1.3$ (e)–(g). (a) $t=0$, (b) $t=350$, (c) $t=800$, (d) $t=0$, (f) $t=140$, (g) $t=400$. Other parameters as in Fig. 1(a).

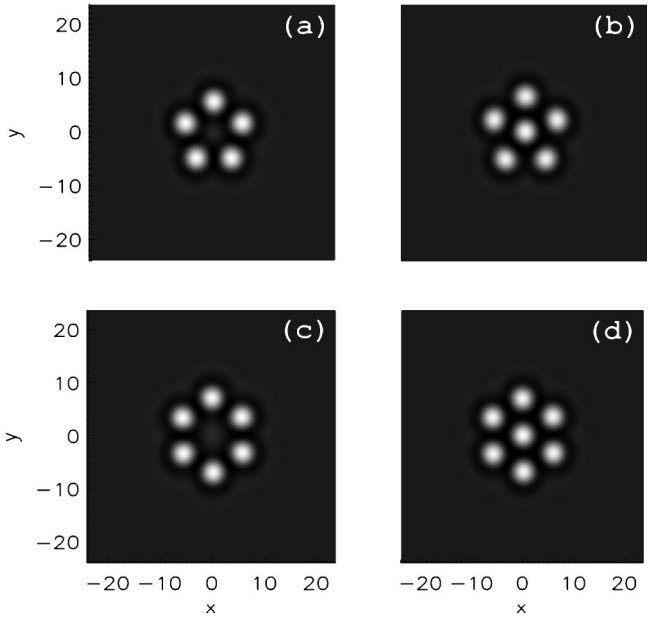

FIG. 10. Stable (a), unstable (b), pentagonal and stable hexagonal (c), (d) clusters found through the Newton method (stability calculated and verified using Arnoldi and split-step method programs). $|E_0|^2=1.3$; other parameters as in Fig. 1(a).

It is worthwhile to stress that the smallest stationary square, i.e., with $d\simeq 6.85$ (very close to the first stable distance found in the pairwise analysis) is actually unstable. It evolves into the rhombus formed by two equilateral triangles [39]. The instability with respect to stretching of the diagonal is the only instability of the smallest square. The next square, with $d\simeq 9.42$ [see Fig. 7(a)] is unstable with respect to all non-neutral degrees of freedom described by Eq. (23). Corresponding eigenmodes are shown in Figs. 7(b)–7(i) and dependencies of the unstable eigenvalues on $|E_0|^2$ are plotted in Fig. 8. They are all smaller than the dominant unstable mode of the corresponding triangle, shown in Fig. 5. The eigenvalues corresponding to the modes depicted in Figs. 7(h)–7(i) are degenerate and very small. The three largest eigenvalues are quite close in value, and correspond to the three modes shown in Figs.7(e)–7(f). Initializing Eqs. (1) with the $d\simeq 9.42$ square one can observe any of the three dominant scenarios of evolution. We find, however, that, in agreement with our stability analysis, at low values of the pump the square first evolves towards the square cluster with $d\simeq 6.85$, which, being itself unstable, eventually transforms into a rhombus, see Figs. 9(a)–9(c) and Ref. [39]. For higher pump values, the dominant scenarios are either evolution towards a trapezoidal structure, see Figs. 9(d)–9(f) or towards a rectangular one. Selection of either of the latter two was found to be highly sensitive to the noise level and to the accuracy of the numerical integration.

The square at $d\simeq 11.93$ is stable, which suggests that a stable square pattern with sufficiently large period exists in this system. Note, that clusters of equilateral triangles naturally form hexagons, which are well known to be dominating pattern in this [5] and many other dissipative systems exhibiting spatial instabilities. Their domination can be in part explained by the rigidity arguments given above for the triangular and rhomboidal clusters.

A major difference between clusters and patterns is that the period of a pattern can be continuously varied within a certain range, when all other parameters of the problem are fixed, see, e.g., Refs. [37,38]. We remark that the (uniquely determined) closest stable distance d of the clusters considered here, see, e.g., Fig. 1, is within the range of lattice constants for stable hexagonal patterns found for the same parameters [38]. Therefore, the potential G seems to be relevant even for large close-packed clusters approaching full patterns. More detailed analysis of the interplay between existence and stability of clusters and corresponding patterns will be the subject of a separate investigation. For earlier approaches to this problem, see, e.g., Refs. [6,12,16]. Apart from the clusters discussed above we have been able to form a rich variety of stable and unstable clusters with $N>4$, four examples of which are shown in Fig. 10.

V. SUMMARY

We have developed asymptotic theory of cluster formation from two-dimensional localized structures of light excited in an externally driven optical cavity with nonlinear absorber. It was shown that these structures interact through forces obeying a linear superposition principle and that they can form various types of clusters. A technique, having applicability beyond the model under consideration, for calculation of the interaction potential through modified Bessel functions, was developed. The stability and instability properties of clusters of two, three, and four cavity solitons have been analyzed in detail using a combination of analytical and numerical methods. A qualitative difference between the stability properties of triangular and square structures was identified and discussed, emphasizing the role of diagonal interactions in the square cluster.

Note added in proof. We acknowledge N. N. Rosanov for noting that isosceles triangles generally move very slowly and their velocity is the order of ϵ^2 or higher, which is not captured by the order of ϵ analyses used above.

ACKNOWLEDGMENTS

This work was largely supported by the UK EPSRC Grant No. GR/N19830 and partially by ESPRIT project 28235 PIANOS. A.G.V. acknowledges support from the Royal Society. The authors are grateful to G.K. Harkness for collaboration in the initial stages of the work.

APPENDIX

Using Eqs. (22) and (20) we obtain

$$\mathbf{I}_n \equiv \left\langle \frac{\mathbf{r}_n}{r_n}\vec{\mathcal{V}}_n \middle| \vec{\mathcal{I}} \right\rangle = \left\langle \frac{\mathbf{r}_n}{r_n}\vec{\mathcal{V}}_n \middle| \vec{\mathcal{I}} \right\rangle_n + \left\langle \frac{\mathbf{r}_n}{r_n}\vec{\mathcal{V}}_n \middle| \vec{\mathcal{I}} \right\rangle_m$$

$$= \left\langle \frac{\mathbf{r}_n}{r_n}\vec{\mathcal{V}}_n \middle| \vec{\mathcal{I}} \right\rangle_n + O(\epsilon^{3/2})$$

$$= \left\langle \frac{\mathbf{r}_n}{r_n}\vec{\mathcal{V}}_n \middle| \hat{\mathcal{L}}(\vec{\psi}_{sn})\vec{\psi}_{sm} \right\rangle_n + O(\epsilon^{3/2})$$

$$= \left\langle \hat{\mathcal{L}}^{\dagger}(\vec{\psi}_{sn})\frac{\mathbf{r}_n}{r_n}\vec{\mathcal{V}}_n \middle| \vec{\psi}_{sm} \right\rangle_n + i\int_{-\infty}^{\infty} dy \int_n dx \left[\left(\frac{\mathbf{r}_n}{r_n}\vec{\mathcal{V}}_n \cdot \hat{\mathcal{D}}\boldsymbol{\nabla}_{\perp}^2 \vec{\psi}_{sm} \right) - \left(\vec{\psi}_{sm} \cdot \hat{\mathcal{D}}\boldsymbol{\nabla}_{\perp}^2 \frac{\mathbf{r}_n}{r_n}\vec{\mathcal{V}}_n \right) \right] + O(\epsilon^{3/2})$$

$$= -i(-1)^n \int_{-\infty}^{\infty} dy \left[\left(\frac{\mathbf{r}_n}{r_n}\vec{\mathcal{V}}_n \cdot \hat{\mathcal{D}}\partial_x \vec{\psi}_{sm} \right) - \left(\vec{\psi}_{sm} \cdot \hat{\mathcal{D}}\partial_x \frac{\mathbf{r}_n}{r_n}\vec{\mathcal{V}}_n \right) \right]_{x=0} + O(\epsilon^{3/2}),$$

with $n,m=1,2$, $m \neq n$, $\int_1 dx = \int_{-\infty}^{0} dx$, and $\int_2 dx = \int_0^{\infty} dx$. Here we have used Green's theorem to transform the integral over the halfplane $(-1)^n x > 0$ into an integral over the y axis. Since the intensity maxima of the two cavity solitons are located symmetrically on the x axis with respect to its origin we have $(\partial_x \vec{\psi}_{sm})_{x=0} = -(\partial_x \vec{\psi}_{sn})_{x=0}$ and $(\vec{\psi}_{sm})_{x=0} = (\vec{\psi}_{sn})_{x=0}$. Using these relations the overlap integral $\mathbf{I}_n$ can be rewritten as

$$\mathbf{I}_n \approx i(-1)^n \int_{-\infty}^{\infty} dy \left[\partial_x \left(\vec{\psi}_{sn} \cdot \frac{\mathbf{r}_n}{r_n}\hat{\mathcal{D}}\vec{\mathcal{V}}_n \right) \right]_{x=0}. \quad \text{(A1)}$$

Substituting into Eq. (A1) the asymptotics (8) and (14), and using the orthogonality conditions $(\hat{\tau}\vec{\mathcal{B}} \cdot \hat{D}\vec{\mathcal{A}}) = (\vec{\mathcal{B}} \cdot \hat{D}\hat{\tau}\vec{\mathcal{A}}) = 0$, we get

$$\mathbf{I}_n \approx i(-1)^n ab \int_{-\infty}^{\infty} dy \left[\partial_x \left(\frac{\mathbf{r}_n}{r_n} K_0(kr_n) K_1(kr_n) \right) \right]_{x=0} - \text{c.c.}$$

$$= 4\pi \frac{\mathbf{R}_{nm}}{R_{nm}} \mathrm{Im}[abK_1(kR_{nm})]$$

$$= -4\pi \boldsymbol{\nabla}_{\mathbf{R}_n} \mathrm{Im}\left[\frac{ab}{k} K_0(kR_{nm}) \right],$$

where $\mathbf{R}_{nm} = \mathbf{R}_n - \mathbf{R}_m$ and $R_{nm} = |\mathbf{R}_{nm}|$ and $n,m=1,2$, $m \neq n$. Here we have used the relation

$$\int_{-\infty}^{\infty} dy \left[\partial_x \left(\frac{\mathbf{r}_n}{r_n} K_0(kr_n) K_1(kr_n) \right) \right]_{x=0} = -2\pi(-1)^n \frac{\mathbf{R}_{nm}}{R_{nm}} K_1(kR_{nm}).$$

[1] M. Saffman, D. Montgomery, and D.Z. Anderson, Opt. Lett. **19**, 518 (1994).

[2] V.B. Taranenko, K. Staliunas, and C.O. Weiss, Phys. Rev. A **56**, 1582 (1997); K. Staliunas, V.B. Taranenko, G. Slekys, R. Viselga, and C.O. Weiss, *ibid.* **57**, 599 (1998).

[3] V.B. Taranenko, I. Ganne, R.J. Kuszelewicz, and C.O. Weiss, Phys. Rev. A **61**, 063818 (2000).

[4] S. Barland, M. Giudici, J. R. Tredicce, L. Spinelli, G. Tissoni, L. A. Lugiato, and M. Brambilla, *Nonlinear Guided Waves and Their Applications*, OSA Technical Digest (Optical Society of America, Washington, D.C., 2001), pp. 2–4.

[5] W.J. Firth and A.J. Scroggie, Phys. Rev. Lett. **76**, 1623 (1996).

[6] W.J. Firth, A. Lord, and A.J. Scroggie, Phys. Scr. **T67**, 12 (1996).

[7] D.V. Skryabin, Phys. Rev. E **60**, R3508 (1999).

[8] S. Longhi, Phys. Rev. E **53**, 5520 (1996); **55**, 1060 (1997).

[9] I.V. Barashenkov, Y.S. Smirnov, and N.V. Alexeeva, Phys. Rev. E **57**, 2350 (1998).

[10] D.V. Skryabin and W.J. Firth, Opt. Lett. **24**, 1056 (1999).

[11] T. Maggipinto, M. Brambilla, G.K. Harkness, and W.J. Firth, Phys. Rev. E **62**, 8726 (2000).

[12] M. Brambilla, L.A. Lugiato, and M. Stefani, Europhys. Lett. **34**, 109 (1996).

[13] B. Schäpers, M. Feldmann, T. Ackemann, and W. Lange, Phys. Rev. Lett. **85**, 748 (2000).

[14] M. Saffman (private communication).

[15] N.N. Rosanov and G.V. Khodova, J. Opt. Soc. Am. B **7**, 1057 (1990); N.N. Rosanov, Prog. Opt. **35**, 1 (1996).

[16] N. N. Rozanov, *Optical Bistability and Hysteresis in Distributed Nonlinear Systems* (Nauka, Moscow, 1997), Chap. 4.

[17] M. Tlidi, P. Mandel, and R. Lefever, Phys. Rev. Lett. **73**, 640 (1994).

[18] I.S. Aranson, K.A. Gorshkov, A.S. Lomov, and M.I. Rabinovich, Physica D **43**, 435 (1990).

[19] P. Coullet, C. Riera, and C. Tresser, Phys. Rev. Lett. **84**, 3069 (2000).

[20] C. Crawford and H. Riecke, Physica D **129**, 83 (1999).

[21] C.P. Schenk, P. Schütz, M. Bode, and H.-G. Purwins, Phys. Rev. E **57**, 6480 (1998).

[22] Yu.A. Astrov and Yu.A. Logvin, Phys. Rev. Lett. **79**, 2983 (1997).

[23] P. Umbanhowar, F. Melo, and H. Swinney, Nature (London) **382**, 793 (1996).

[24] B.A. Malomed, Phys. Rev. E **58**, 7928 (1998).

[25] B.A. Malomed, Phys. Rev. A **44**, 6954 (1991).

[26] V.V. Afanasjev, B.A. Malomed, and P.L. Chu, Phys. Rev. E **56**, 6020 (1997).

[27] N.N. Akhmediev, A. Ankiewicz, and J.M. Soto-Crespo, Phys. Rev. Lett. **79**, 4047 (1997); J.M. Soto-Crespo and N.N. Akhmediev, J. Opt. Soc. Am. B **16**, 674 (1999).

[28] A.G. Vladimirov, G.V. Khodova, and N.N. Rosanov, Phys. Rev. E **63**, 056607 (2001).

[29] A.V. Mamaev, A.A. Zozulya, V.K. Mezentsev, D.Z. Anderson, and M. Saffman, Phys. Rev. A **56**, R1110 (1997).

[30] W. Krolikowski, E.A. Ostrovskaya, C. Weilnau, M. Geisser, G. McCarthy, Y.S. Kivshar, C. Denz, and B. Luther-Davies, Phys. Rev. Lett. **85**, 1424 (2000).
[31] M. Soljacic, S. Sears, and M. Segev, Phys. Rev. Lett. **81**, 4851 (1998).
[32] A.S. Desyatnikov and Y.S. Kivshar, Phys. Rev. Lett. **87**, 033901 (2001).
[33] A.V. Buryak, Y.S. Kivshar, M.F. Shih, and M. Segev, Phys. Rev. Lett. **82**, 81 (1999).
[34] J. Schjodt-Eriksen, M.R. Schmidt, J.J. Rasmussen, P.L. Christiansen, Y.B. Gaididei, and L. Berge, Phys. Lett. A **246**, 423 (1998).
[35] D.V. Skryabin, A.R. Champneys, and W.J. Firth, Phys. Rev. Lett. **84**, 463 (2000).
[36] R. B. Lehoucq, D. C. Sorensen, and C. Yang, *Solutions of Large Scale Eigenvalue Problems with Implicitly Restarted Arnoldi Methods* (Rice University, Houston, 1997), http://www.caam.rice.edu/software/ARPACK/
[37] P.K. Jakobsen, J. Lega, Q. Feng, M. Staley, J.V. Moloney, and A.C. Newell, Phys. Rev. A **49**, 4189 (1994).
[38] G. K. Harkness, W. J. Firth, and G.-L. Oppo, International Quantum Electronics Conference, Nice, 2000, Conference Digest (IEEE Catalog No. 00TH8504), p. 47.
[39] Movies in the mpg format visualizing dynamics of clusters can be downloaded from http://staff.bath.ac.uk/pysdvs/ and http://cnqo.phys.strath.ac.uk/movies/